analytical chemistry

Article

Cite This: Anal. Chem. XXXX, XXX, XXX−XXX

pubs.acs.org/ac

Quantitative Imaging of Lipid Synthesis and Lipolysis Dynamics in *Caenorhabditis elegans* by Stimulated Raman Scattering Microscopy

Xuesong Li,[†,‡,⊥] Yan Li,[§,⊥] Meijuan Jiang,[∥,⊥] Wanjie Wu,[†,‡] Sicong He,[†,‡] Congping Chen,[†,‡] Zhongya Qin,[†,‡] Ben Zhong Tang,[∥] Ho Yi Mak,[*,§] and Jianan Y. Qu[*,†,‡]

[†]Department of Electronic and Computer Engineering, Hong Kong University of Science and Technology, Clear Water Bay, Kowloon, Hong Kong 999077, China

[‡]Center of Systems Biology and Human Health, School of Science and Institute for Advanced Study, Hong Kong University of Science and Technology, Clear Water Bay, Kowloon, Hong Kong 999077, China

[§]Division of Life Science, Hong Kong University of Science and Technology, Clear Water Bay, Kowloon, Hong Kong 999077, China

[∥]Department of Chemistry, Hong Kong University of Science and Technology, Clear Water Bay, Kowloon, Hong Kong 999077, China

Supporting Information

ABSTRACT: Quantitative methods to precisely measure cellular states in vivo have become increasingly important and desirable in modern biology. Recently, stimulated Raman scattering (SRS) microscopy has emerged as a powerful tool to visualize small biological molecules tagged with alkyne (C≡C) or carbon−deuterium (C−D) bonds in the cell-silent region. In this study, we developed a technique based on SRS microscopy of vibrational tags for quantitative imaging of lipid synthesis and lipolysis in live animals. The technique aims to overcome the major limitations of conventional fluorescent staining and lipid extraction methods that do not provide the capability of in vivo quantitative analysis. Specifically, we used three bioorthogonal lipid molecules (the alkyne-tagged fatty acid 17-ODYA, deuterium-labeled saturated fatty acid PA-D_{31}, and unsaturated fatty acid OA-D_{34}) to investigate the metabolic dynamics of lipid droplets (LDs) in live *Caenorhabditis elegans* (*C. elegans*). Using a hyperspectral SRS (hsSRS) microscope and subtraction method, the interfering non-Raman background was eliminated to improve the accuracy of lipid quantification. A linear relationship between SRS signals and fatty acid molar concentrations was accurately established. With this quantitative analysis tool, we imaged and determined the changes in concentration of the three fatty acids in LDs of fed or starved adult *C. elegans*. Using the hsSRS imaging mode, we also observed the desaturation of fatty acids in adult *C. elegans* via spectral analysis on the SRS signals from LDs. The results demonstrated the unique capability of hsSRS microscopy in quantitative analysis of lipid metabolism in vivo.

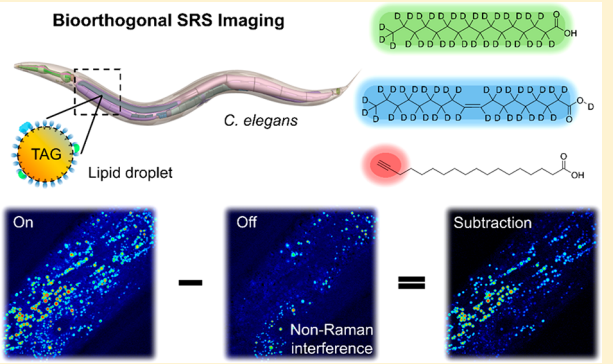

Lipids, encompassing molecules such as fatty acids and their derivatives as well as sterol-containing metabolites, are essential for cell structure and function. For example, fatty acids in the form of triglycerides (TAG) are mainly stored in lipid droplets (LDs), a conserved organelle for fat storage. Phospholipids are the main constituents of the cell membranes that segregate biochemical reactions in stable compartments. More recent studies have shown that they are also involved in the regulation of intracellular signaling pathways, transcription factor activity, and gene expression.[1] In obesity, fatty liver disease, type 2 diabetes, and cancer, abnormal accumulation or turnover of lipids contribute significantly to cellular dysfunction.[2−4] To determine steady-state lipid levels, conventional methods including lipid extraction,[5] transmission electron microscopy (TEM),[6] lipophilic dye staining,[7] and genetically encoded fluorescent proteins for labeling LDs[8] have been developed and widely used. However, lipid extraction by organic solvent is detrimental to live samples. TEM can distinguish LDs from other organelles based on their phospholipid monolayer surface at nanoscale resolution, but it requires sample fixation and complex processing procedures. The accuracy of dye staining methods based on Nile Red and BODIPY are highly dependent on methods used for sample preparation.[7,9] Fluorescent dyes are sensitive to environmental changes, which may hinder their use for lipid quantification.[10] Though transgenic expression of fluorescent proteins at LDs surface significantly improves the accuracy of LDs detection, the use of such fluorescent markers are limited to specific

Received: October 24, 2018
Accepted: December 27, 2018
Published: December 27, 2018

DOI: 10.1021/acs.analchem.8b04875
Anal. Chem. XXXX, XXX, XXX−XXX

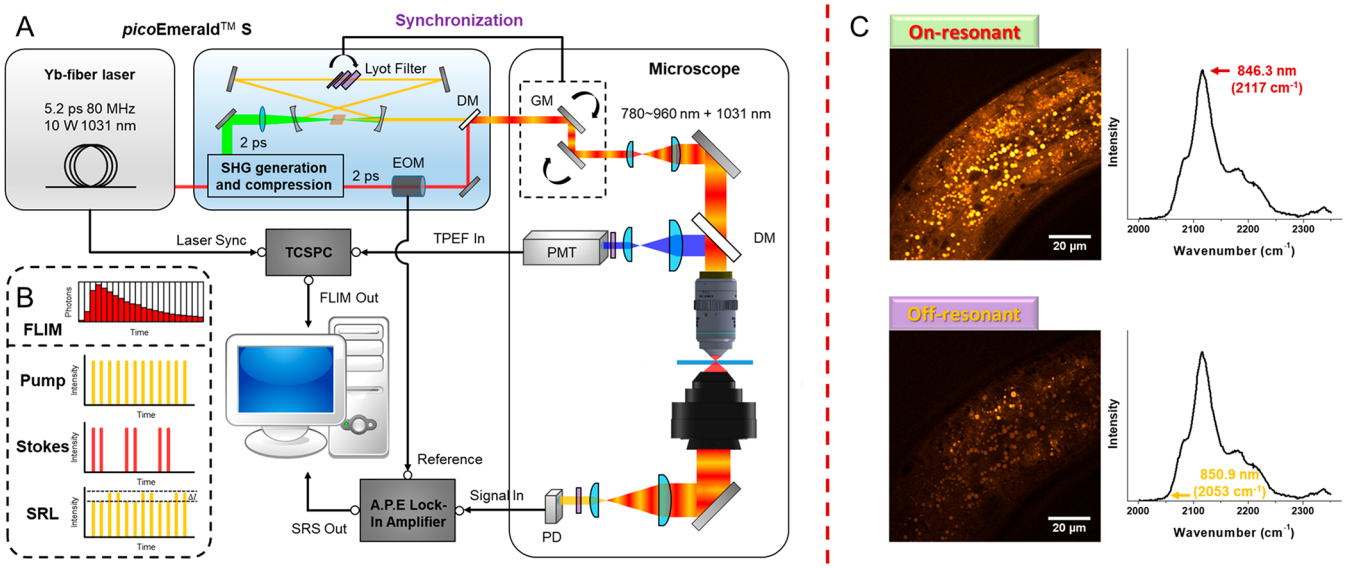

Figure 1. SRS imaging of Raman-bioorthogonal fatty acids in *C. elegans*. (A) Schematic diagram of the hsSRS microscope. Fast wavelength tuning of the pump beam can be performed by synchronizing the Lyot filter to the microscope frame trigger. SHG, second-harmonic generation; EOM, electro-optical modulator; DM, dichroic mirror; GM, galvanometer scanner; PMT, photomultiplier tube; PD, photodiode; TPEF, two-photon excited fluorescence; FLIM, fluorescence lifetime imaging; TCSPC, time-correlated single photon counting; SRL, stimulated Raman loss. (B) Schemes of FLIM and SRL detection principles. TCSPC records times at which individual photons are detected by the PMT with respect to the excitation laser pulse, and recordings are repeated for multiple laser pulses to form a fluorescence decay curve. The Stokes beam is modulated at high frequency (20 MHz), at which the resulting amplitude modulation of the pump beam due to SRL can be detected by the lock-in amplifier. (C) SRS spectrum of deuterium-labeled saturated palmitic acid PA-D_{31} and SRS images of one worm fed with PA-D_{31} at 2117 cm^{-1} (on-resonant) and 2053 cm^{-1} (off-resonant) Raman shifts in situ, respectively.

tissues.[8,11] Therefore, the limitations of these conventional methods motivate the development of in vivo quantitative measurement of lipids in living organism.

In recent years, vibrational microscopy has been widely used for noninvasive detection of lipids in cells. Different from fluorescence, vibrational microscopy distinguishes the cellular components by the Raman spectral signatures of endogenous molecules. A number of studies have utilized the spectral features of aliphatic methylene groups ($-CH_2$) in fatty acids to visualize endogenous lipids via spontaneous Raman microscopy,[12] coherent anti-Stokes Raman scattering (CARS) microscopy,[13] and stimulated Raman scattering (SRS) microscopy.[10,14,15] Among them, SRS microscopy is superior to spontaneous Raman microscopy for its higher spatial resolution and 10^4 times faster image acquisition speed, owing to its nonlinear optical process.[14,15] It is also free from nonresonant background and well resembles the spontaneous Raman spectrum when compared with CARS.[14] These advantages are particularly critical in LDs study because their structures are highly dynamic and their size may vary considerably from fibroblasts (100−200 nm) to white adipocytes (up to 100 μm).[2,16] Moreover, SRS intensity has linear dependence on the amount of selected chemical bonds at focal volume, which makes it ideal to image and analyze the amount of lipids stored in organisms quantitatively.[10,17,18]

In Raman imaging, chemical modification of the targeting molecule by tagging a Raman probe with stable isotopes or alkyne bonds can further enhance the detection sensitivity and specificity.[19−30] Compared to most fluorophores, these Raman tags are small, structurally stable, and unsusceptible to photobleaching, enabling continuous live cell imaging.[31] In particular, the substitution of hydrogen by heavier deuterium results in carbon-deuterium (C−D) bonds with a lower stretching frequency at 2000−2400 cm^{-1}.[19] Alkyne tags or carbon−carbon triple bonds (C≡C) exhibit Raman signal at ~2120 cm^{-1} with large Raman cross sections.[24] These Raman tags all have the vibrational frequencies located in the cell-silent region from 1800 to 2800 cm^{-1}, where the endogenous Raman signal is considerably low. Previous studies have demonstrated that these bioorthogonal Raman tags offered an exciting opportunity to distinguish newly formed lipids from endogenous ones,[21,26,27,32−35] and the combination of bioorthogonal fatty acids and SRS microscopy is a promising and powerful approach for the study of lipid metabolic processes.[26,27,33−36]

However, SRS microscopy is not absolutely free of interference signals. In solution, SRS spectrum is accompanied by broad background baseline resulting from competing four-wave mixing and pump−probe processes.[31,37] Moreover, in biological samples, complex interactions between the laser and microenvironment will introduce other unwanted heterodyne contrast in SRS imaging, including cross-phase modulation, transient absorption, and thermal lens effect.[38] Different from the nonresonant background of CARS due to the third-order susceptibility, these interference signals are regarded as "non-Raman background" of SRS. Therefore, to perform the quantitative SRS imaging of lipid metabolic process in vivo, an accurate calibration curve between the SRS intensity and the amount of lipids must be built by removing the concomitant interferences in the measured SRS signal. In this work, we introduced a method to eliminate the non-Raman background and obtained the equivalent molar concentration levels of bioorthogonal fatty acids in *Caenorhabditis elegans* (*C. elegans*) in vivo with high spatial resolution (Figure 1, and Supporting Information, Figure S1). Specifically, two deuterium-labeled fatty acids, deuterated palmitic acid (PA-D_{31}) and deuterated oleic acid (OA-D_{34}), were chosen as representative deuterated probes, in which palmitic

DOI: 10.1021/acs.analchem.8b04875
Anal. Chem. XXXX, XXX, XXX−XXX

acid (C16:0) is one of the most common saturated fatty acids (SFAs) and oleic acid (C18:1) is the most abundant *cis* monounsaturated fatty acid (MUFA) in wild-type *C. elegans*.[39] One alkyne-tagged fatty acid, 17-octadecynoic acid (17-ODYA), was used as representative alkyne-tagged probe, and it was used as the palmitoylation reporter in previous studies.[40,41]

C. elegans is a commonly used animal model for studying the lipid or fat metabolism. Most of its body fat are stored in the intestine in the form of LDs, which vary in size and number dependent on nutritional status. To eliminate the concomitant interferences, we used a method, named SRS subtraction, to obtain the genuine signal I_{SRS} by the subtraction of its off-resonant signal (I_{OFF}) from the on-resonant signal (I_{ON}). We found that the retrieved SRS signal ($I_{SRS} = I_{ON} - I_{OFF}$) was proportional to the concentration with good linearity and negligible intercepts. With a calibration technique, we further quantitatively measured the accumulation and dissipation of bioorthogonal fatty acids in live *C. elegans* that were fed ad libitum and under starvation. In *C. elegans*, the lysosome-related organelles (LROs) produce similar features as LDs in SRS imaging and have often caused difficulties in accurate identification of LDs.[42] Fortunately, the interference from LROs can also be eliminated by SRS subtraction to improve the accuracy in LDs detection and characterization. Finally, we revealed the desaturation of fatty acids in adult *C. elegans* using the hyperspectral imaging mode of our SRS microscope system, demonstrating the great potential of hyperspectral SRS (hsSRS) microscopy in the study of important lipid conversion processes in vivo.

EXPERIMENTAL SECTION

Hyperspectral SRS Microscopy. The hsSRS microscope (Figure 1A) was described in detail in our recent paper.[43] Briefly, an integrated optical parametric oscillator (OPO, *pico*Emerald S, APE) was used as the light source for both pump and Stokes beams. It provided two synchronized pulse trains (Stokes beam, 1031 nm; pump beam, tunable from 780 to 960 nm) with 2 ps pulse duration and 80 MHz repetition rate. The intensity of the 1031 nm Stokes beam was modulated by a built-in electro-optical modulator at 20 MHz. After collimation, magnification, and power regulation, two beams were directed into a homemade laser scanning microscope. A 40× water immersion objective (UAPO40XW3/340, 1.15 NA, Olympus) and oil immersion condenser (UAAC, 1.4 NA, Olympus) was used throughout this study following Köhler illumination. After blocking the Stokes beam, the pump beam was detected by a fast Si-photodiode and a lock-in amplifier. The hsSRS imaging mode and two-wavelength SRS subtraction method are described in detail in the Supporting Information.

***C. elegans* Strains and Culture.** N2 Bristol strains were grown on standard nematode growth media (NGM) plates seeded with OP50 *Escherichia coli* at 20 °C using standard protocols. *C. elegans* were anesthetized in 0.2 mM levamisole prior to being mounted on 8% agarose pads on microscope slides immediately before SRS imaging.

Deuterated and Alkyne-Tagged Fatty Acid Supplementation. For *C. elegans* fatty acid supplementation, OP50 bacterial culture was first mixed well with 4 mM PA-D_{31} or OA-D_{34} or 17-ODYA (366897, 683582, and O8382, Sigma) and then seeded onto NGM plates. To measure fatty acid accumulation, populations of young adults, raised in the absence of deuterated and alkyne-tagged fatty acid were transferred to plates with PA-D_{31} or OA-D_{34} or 17-ODYA, respectively. To measure basal fat turnover, populations of synchronized L1 larvae were raised on OP50 seeded plates with PA-D_{31} or OA-D_{34} or 17-ODYA, and when grown to young adults, they were transferred to OP50 seeded plates without deuterated and alkyne-tagged fatty acids. The worm starvation experiment was similar to the one that measured lipid turnover, but young adults were transferred to NGM plates without any food. Worms were imaged by SRS at 5−6 h intervals for over 30 h. In each worm, we mainly focused on the first two segments of intestinal cells in the anterior region and the average signal intensity of intestinal LDs was measured.

RESULTS AND DISCUSSION

SRS Properties of Bioorthogonal Fatty Acids. The chemical structures of PA-D_{31}, OA-D_{34}, and 17-ODYA are shown in Figure 2A, and their functional Raman moieties are marked with various colors (green for PA-D_{31}, blue for OA-D_{34}, and red for 17-ODYA). First, we calculated their theoretical Raman spectra in gas phase using Gaussian 09 program and measured their hsSRS spectra in solutions (Figure 2B,C). PA-D_{31} and OA-D_{34} both had a sharp C−D

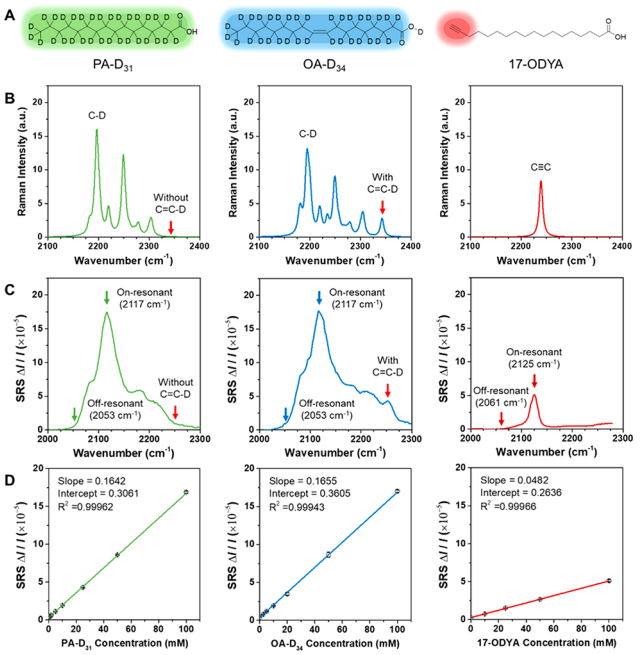

Figure 2. SRS properties of three Raman-bioorthogonal fatty acids. (A) Chemical structures of PA-D_{31}, OA-D_{34}, and 17-ODYA. The functional groups of Raman tags are marked in green, blue, and red, respectively. (B) Theoretically calculated Raman spectra using Gaussian 09 program. The calculations were performed at vacuum gas phase via ground state DFT at the basis set of B3LYP/6-31g (d, p). (C) hsSRS spectra of 100 mM PA-D_{31}, OA-D_{34}, and 17-ODYA solutions. Spectral intensity was acquired from lock-in amplifier output directly and subtracted by the concurrent non-SRS background signals that have a flat spectral response. Spectral acquisition time: 4 s/point. (D) SRS intensity versus concentration plots of three different fatty acid solutions. SRS intensity was calculated based on the subtraction of off-resonant background from on-resonant signals marked in (C). Data acquisition speed: 25.6 μs/pixel. Data represents the mean ± SD in more than five measurements.

DOI: 10.1021/acs.analchem.8b04875
Anal. Chem. XXXX, XXX, XXX−XXX

Raman peak at 2197 cm^{-1} with fine structures induced by different vibrational modes, whereas OA-D_{34} had an additional C═C−D peak at 2343 cm^{-1}. 17-ODYA had a single C≡C Raman peak at 2239 cm^{-1} (Figure 2B). Compared with the spectral data in gas phase, molecules in solution are hindered rotors affected by solvent effects, mainly the collisions, and thus they do not show discrete rotational levels.[44] Broad bands were observed for molecules in solution with few fine structures and a solvent-induced red-shift of line maxima (Figure 2C). This can be explained by that the experimentally measured SRS line shape is a convolution of intrinsic one with solvent-induced broadening function.[45] Although the calculated sharp C−D peak of PA-D_{31} in gas phase was more intense than that of OA-D_{34} (Figure 2B), the two fatty acid probes produced similar SRS C−D peak intensities at 2117 cm^{-1} in solutions (Figure 2C). From theoretical results, their Raman peak areas around the C−D peak were almost the same (PA-D_{31}, 291 au, and OA-D_{34}, 309 au; Supporting Information, Table S1), suggesting that they possessed similar vibrational energies from C−D bonds and resulted in SRS intensities at 2117 cm^{-1} in solutions after solvent-induced spectral broadening and shifting.

Spectroscopically, PA-D_{31} and OA-D_{34} had similar SRS spectral profiles with the strongest signal detected at 2117 cm^{-1}, and OA-D_{34} could be distinguished from PA-D_{31} by the less pronounced Raman peak at 2252 cm^{-1} (Figure 2C), which was attributed to the unsaturated C═C−D stretches from the theoretical calculations (Figure 2B) and spontaneous Raman analysis.[21] The full width at half-maximum (fwhm) of PA-D_{31} and OA-D_{34} was measured to be 47.5 and 60 cm^{-1}, respectively. In contrast, alkyne-tagged 17-ODYA had a sharp Raman peak at 2125 cm^{-1} with a much narrower fwhm of 16 cm^{-1}. The C≡C bond is believed to be superior to C−D bonds for cell-silent vibrational imaging because of the higher Raman intensity per tag.[26] It could be calculated that the Raman intensity for a single terminal C≡C was about 9-fold higher than that of one C−D bond (Figure 2C,D), which is consistent with the previous report.[25] Nevertheless, from the molecular aspect, PA-D_{31} and OA-D_{34} possessed a more than 3.5-fold stronger SRS signal per molecule than 17-ODYA because there are 31 C−D bonds in PA-D_{31} and 33 in OA-D_{34} but only one terminal alkyne bond in 17-ODYA. This thus improves the signal-to-noise ratio (SNR) of PA-D_{31} or OA-D_{34} in SRS imaging.

Non-Raman backgrounds, including cross-phase modulation, transient absorption, and thermal lensing effects, are often found in SRS imaging and can severely deteriorate SRS signals both in the fingerprint and cell-silent vibrational regions.[38] Owing to the narrow spectral profiles of these fatty acids in the cell-silent region, we could easily obtain their genuine SRS intensity ($I_{SRS} = I_{ON} - I_{OFF}$) by subtracting their SRS baseline signal (off-resonant, I_{OFF}) from their SRS peak signal (on-resonant, I_{ON}), which is 60 to 70 cm^{-1} away from their Raman peaks, to remove the non-SRS signals. In our previous work, this SRS subtraction method was demonstrated to efficiently suppress the non-Raman backgrounds and be capable of imaging the analyte of interest with high contrast and direct measurement of concentration.[43] In principle, by keeping the same laser excitation and signal recording conditions, calibration curves can be built to calculate the in situ concentration of Raman-tagged fatty acids owing to the linear concentration dependence and inert environmental sensitivity of SRS signals.[43]

SRS Calibrations for Concentration Measurement. We introduce the details of SRS measurement in live *C. elegans* and quantitative calculation of the equivalent concentration of the bioorthogonal fatty acids in LDs. The "on-resonant" and "off-resonant" wavenumbers were set to 2117 and 2053 cm^{-1} for PA-D_{31} and OA-D_{34} and 2125 and 2061 cm^{-1} for 17-ODYA, respectively (Figure 2C). The calibration curves of the I_{SRS} and the fatty acid concentration c were obtained as I_{SRS} = slope × c + intercept with very high linear coefficients of >0.999 (Figure 2D). The wavenumber difference between on- and off-resonant signals was determined by the maximal tuning range of the pump laser in fast-wavelength-sweeping mode. The slopes of the three fatty acids were calculated to be 0.1642 for PA-D_{31}, 0.1655 for OA-D_{34}, and 0.0482 for 17-ODYA (unit: 10^{-5}/mM), respectively, and their detection limits were calculated to be 0.48, 0.45, and 1.56 mM, respectively, reflecting the detection sensitivity of our homemade SRS system for these bioorthogonal fatty acids. The intercepts of the fitting curves were close to zero. Therefore, simplified calibrations of $I_{PA\text{-}D31} = 0.1642 \times c$, $I_{OA\text{-}D34} = 0.1655 \times c$, and $I_{17\text{-}OYDA} = 0.0482 \times c$ were obtained and further applied to interpret the equivalent intracellular concentration of the fatty acids measured in live *C. elegans* under the same measurement conditions, and it should be pointed out that the off-resonant wavenumber for PA-D_{31} and OA-D_{34} is not completely located outside their SRS spectra (Figure 2C) due to the limited tuning range of pump laser in fast-wavelength-sweeping mode. However, it caused negligible error in their concentration calibrations (Figure 2D, and Supporting Information, Figure S2).

Because the bioorthogonal fatty acids might be involved in the complex fatty acid metabolism, the final profile of lipids would be complicated in live animals. For example, a group of enzymes, such as FAT-5, FAT-6, and FAT-7, are mainly responsible for desaturation of different kinds of fatty acids.[9,46] Certain proteins can also work together to elongate and desaturate SFA precursors into long-chain polyunsaturated fatty acids (PUFAs).[47] On the basis of the theoretical calculations of 25 types of common fatty acids in diets and *C. elegans*,[1,39] we found that their Raman areas around C−D peak were highly proportional to the number of their C−D bonds regardless of their fatty acid types (Supporting Information, Table S1 and Figure S3), indicating that each C−D produces similar signal at the C−D peak. This was also supported by experimental results of PA-D_{31} and OA-D_{34} and their I_{SRS} at 2117 cm^{-1} per C−D were calculated to be 5.30 × 10^{-8} and 5.02 × 10^{-8} mM^{-1}, respectively. Therefore, the experimental SRS intensity I_{SRS} could well reflect the total concentration of the existing C−D in *C. elegans*. Meanwhile, for 17-ODYA, I_{SRS} at 2125 cm^{-1} reflected the total concentration of the existing alkyne bond. Given the intracellular complexity, it should be noted that the concentrations presented in following experiments were equivalent concentrations of the fatty acids estimated by 31 C−D bonds for PA-D_{31}, 33 C−D bonds for OA-D_{34}, and 1 C≡C bond for 17-ODYA.

SRS Imaging of Bioorthogonal Fatty Acids in *C. elegans*. Next, in vivo SRS imaging was conducted for the three fatty acid probes in *C. elegans*. We performed single-layer scanning to obtain the SRS image and minimize the motion artifacts throughout the study. The imaging depth was located at 6−8 μm away from the coverslip for all animals to maintain

DOI: 10.1021/acs.analchem.8b04875
Anal. Chem. XXXX, XXX, XXX−XXX

the data consistency (Supporting Information, Movie S1, Movie S2, and Figure S4).

Taking 17-ODYA as an example, a worm was fed with 17-ODYA cultured *E. coli* for 15 h before imaging. As shown in Figure 3A,B, a group of on-resonant and off-resonant alkyne

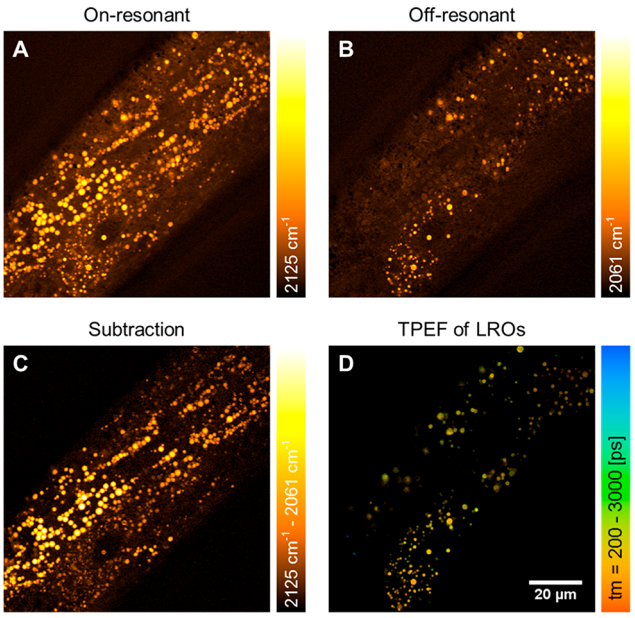

Figure 3. Identification and removal of non-Raman background interference using SRS subtraction method. (A) On-resonant SRS image of *C. elegans* fed with 17-ODYA for 15 h. (B) Off-resonant SRS image at the same site. (C) Subtraction SRS image based on (A) and (B). (D) Color-coded TPEF lifetime image of the autofluorescence from LROs.

SRS images were acquired. After signal subtraction pixel by pixel and intensity normalization, a new SRS image was generated with a higher contrast (Figure 3C). Contrary to the expectation that an off-resonant SRS image should be totally background-free, non-negligible signals were detected in the off-resonant image, which are considered as non-Raman interference in SRS imaging. To further explore the origin of these interference signals, we conducted TPEF lifetime imaging in situ using only the pump beam. The color-coded lifetime image (Figure 3D) shows that these vesicles emitted strong autofluorescence with a short lifetime (<0.9 ns) and colocalized well with the non-Raman signals in Figure 3B. On the basis of our previous work,[42] these interference signals could be attributed to the transient absorption of prevalent LROs in the *C. elegans* intestine. Because the essence of the transient absorption effect is electronic transitions, the non-Raman interference has weak wavelength dependence.[38] The SRS subtraction method could, therefore, effectively eliminate the interference of the LROs, as shown in Figure 3C. This is critical to improve the accuracy of the LDs quantification. Similar results were also obtained in in vivo SRS imaging of *C. elegans* when using deuterated fatty acids PA-D_{31} and OA-D_{34} (Supporting Information, Figures S5 and S6).

Quantitative Analysis of Bioorthogonal Fatty Acids in *C. elegans*. We then traced the accumulation of the bioorthogonal labels over time, as shown in Supporting Information, Figure S7. In eukaryotic cells, fatty acids from de novo synthesis or the diet can be stored as TAG in LDs (Figure 4A). In this study, we focused on the latter pathway. After incubation over different periods of time, we conducted SRS imaging of the bioorthogonal fatty acids and endogenous lipid in the anterior region (first two segments of intestinal cells) of live *C. elegans*, respectively. Using OA-D_{34} as an example, C−D SRS images of *C. elegans* clearly show the distribution of bioorthogonal fatty acids in the *C. elegans* (Figure 4B). With the increasing of incubation time from 0 to 30 h, the SRS signal of bioorthogonal fatty acids gradually increased in LDs, indicating the accumulation of bioorthogonal fatty acids over time. The colocalization of C−D and endogenous $-CH_2$ SRS signals verified that the bioorthogonal fatty acids were mainly stored in LDs (Supporting Information, Figures S8−S10). On the other hand, worms grown on standard OP50 did not show significant intensity changes over time (Supporting Information, Figure S11). In addition, endogenous $-CH_2$ SRS images were captured to measure the size distribution of LDs (Supporting Information, Figure S12).[7] The statistical results showed that feeding with PA-D_{31}, OA-D_{34}, and 17-ODYA had little effects on the LDs size distribution in worms within the tracing time (Supporting Information, Figure S13).

On the basis of the quantitative SRS imaging, we measured the fatty acid accumulation in LDs over time (Supporting Information, Figure S14). Using the concentration calibration obtained in solutions, the average SRS intensity for each time point was calculated and interpreted into the equivalent concentration of a specific bioorthogonal fatty acid, as shown in Figure 4C. Similar to the spontaneous Raman results in THP-1 macrophages,[21] our quantitative SRS data in *C. elegans* also reflected a continuous increase in bioorthorgonal fatty acid storage. Interestingly, the three fatty acids exhibited distinct rates of accumulation in LDs, which implied that PA-D_{31}, OA-D_{34}, and 17-ODYA metabolism may not be homogeneous via the variety of lipid-metabolic pathways that regulate de novo synthesis and transformation of fatty acids.[33] To simplify the analysis, the data were divided into two parts at the node of 15 h, and the accumulation rates were calculated by linear approximation (Supporting Information, Figures S15 and S16 and Table S2). In the first 15 h, the accumulation rate of saturated fatty acid PA-D_{31} (5.28 mM/h) was significantly lower than those of unsaturated fatty acids OA-D_{34} (15.22 mM/h) and 17-ODYA (9.07 mM/h). From 15 to 30 h, the accumulation of PA-D_{31} kept at a steady rate of 6.16 mM/h, whereas the accumulation rate of OA-D_{34} and 17-ODYA slowed down to 6.67 and 3.26 mM/h, respectively. Such a result is consistent with the recent report that the accumulation rate of OA-D_{34} will gradually decrease after 10 h of incubation.[35] Regarding the slowdown of the accumulation rate, it is expected that after long pulse time the labeled lipid concentration will increase. However, their turnover rates will increase as well. The slowdown of uptake or total accumulation rate suggests that the turnover rate increases as the increase of labeled lipid concentration in LDs. Although the accumulation in the posterior region showed a similar trend (Supporting Information, Figure S17), the accumulation concentrations were always lower than those in the anterior region at the same time point, perhaps reflecting the preference for intestinal fat absorption at the anterior region. On the basis of the results of in vivo quantitative imaging, we were able to conclude that oleic acid (C18:1), rather than 17-ODYA and palmitic acid (C16:0), was preferentially accumulated in LDs, suggesting that the lipid-synthesizing enzymes in *C. elegans* might have preference for their substrates,[48] and oleic acid can

DOI: 10.1021/acs.analchem.8b04875
Anal. Chem. XXXX, XXX, XXX−XXX

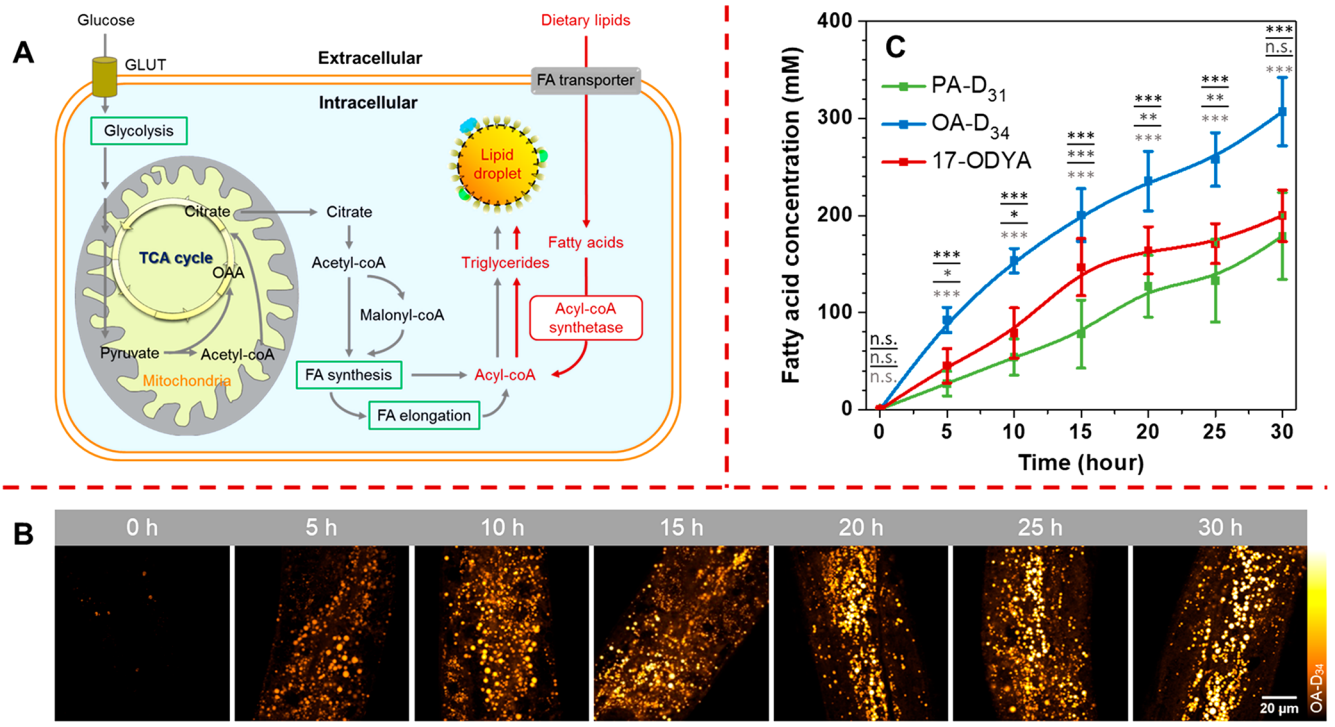

Figure 4. Accumulation rate of different bioorthogonal fatty acids in wild-type *C. elegans*. (A) Scheme of lipid synthesis pathways in eukaryotic cells (gray, glucose-derived de novo lipid synthesis; red, direct uptake of dietary fatty acid). (B) Representative SRS images of OA-D_{34} in worms over different incubation times. (C) Quantitative measurement of fatty acid accumulation dynamics in the anterior region of worms ($n > 12$). Data are represented as mean ± SD. Unpaired, two-tailed *t* test was performed to determine significance (first row, PA-D_{31} and OA-D_{34}; second row, PA-D_{31} and 17-ODYA; third row, OA-D_{34} and 17-ODYA). *, $P < 0.05$; **, $P < 0.01$; ***, $P < 0.001$.

be most efficiently used as the building block of TAG in *C. elegans*.

Basal Fat Turnover and Consumption during Starvation in *C. elegans*. After the study of lipid accumulation, experiments on basal fat turnover and lipid consumption during worm starvation were also conducted. The worms were incubated from L1 larvae to young adults with bioorthogonal fatty acids over certain periods of time (Supporting Information, Figure S18). Then the medium was replaced using normal *E. coli* without C−D or alkyne supplementation to measure basal fat turnover. As a comparison, to study the lipid consumption during starvation, no food supply was provided to these labeled worms as a test group. According to the lipid turnover and lipolysis pathways (Figure 5A), the fatty acids are released by the lipolysis of TAGs and then consumed through mitochondrial *β*-oxidation to supply energy for maintenance of the physiological activities.

First, to study basal fatty acid turnover, we monitored the SRS signals in the anterior region of live *C. elegans* at different time points (Supporting Information, Figures S19−S21) and plotted the equivalent fatty acid concentration over time (Figure 5B). The plot in Figure 5B shows that the equivalent concentrations of bioorthogonal fatty acids all gradually decreased with time in a similar trend, and the labeled lipid turnover rate of the first 10 h was obviously faster than in the next 18 h (Figure 5B, Supporting Information, Figures S22 and S23 and Table S3) because lipids carrying deuterium or alkyne labeling were constantly diluted during the lipid turnover process. Statistical analysis indicated that the average size of LDs was not affected by these fatty acids with time (Supporting Information, Figure S24), demonstrating that lipid efflux, rather than the increase in LDs size, is the main cause of the decreased equivalent concentrations over time. It is important to point out that a previous study based on cell line (THP-1) did not observe a significant signal decrease or intracellular distribution change of PA-D_{31} and OA-D_{34}, leading to the conclusion that the fatty acids were not biochemically degraded or transported out of the cells.[21] However, our current results at the organismal level demonstrated that lipid influx and efflux were reversible for all three bioorthogonal fatty acids.

Second, we studied the lipid consumption by measuring the equivalent concentrations of labeled fatty acids during worm starvation. The equivalent concentrations were all decreased over time in worms (Figure 5C), and their LDs numbers and sizes decreased as expected during the starvation (Supporting Information, Figures S25−S28). However, their lipolysis patterns were different from the corresponding curves when undergoing basal fat turnover (Figure 5C). At the first 5 h of starvation, the decrease in the labeled lipid concentrations was much slower than that during basal lipid turnover. This result is consistent with short-term starvation-induced fat accumulation as observed from cell lines.[49] As reported, such a short-term starvation-induced fat storage plays important roles in reducing the lipotoxicity, maintaining normal mitochondria function and releasing lipid-induced ER stress.[49,50] Nevertheless, the temporarily stored fatty acids in the worms dissipated at a faster rate over longer-time starvation and were exhausted after 20 h. It should be emphasized that we were only measuring the concentration of the labeled fatty acids. Preferential lipolysis of TAG that contains the labeled fatty acid, relative to other endogenous fatty acids, could account for the decrease in the concentration of labeled lipids during worm starvation.[51]

DOI: 10.1021/acs.analchem.8b04875
Anal. Chem. XXXX, XXX, XXX−XXX

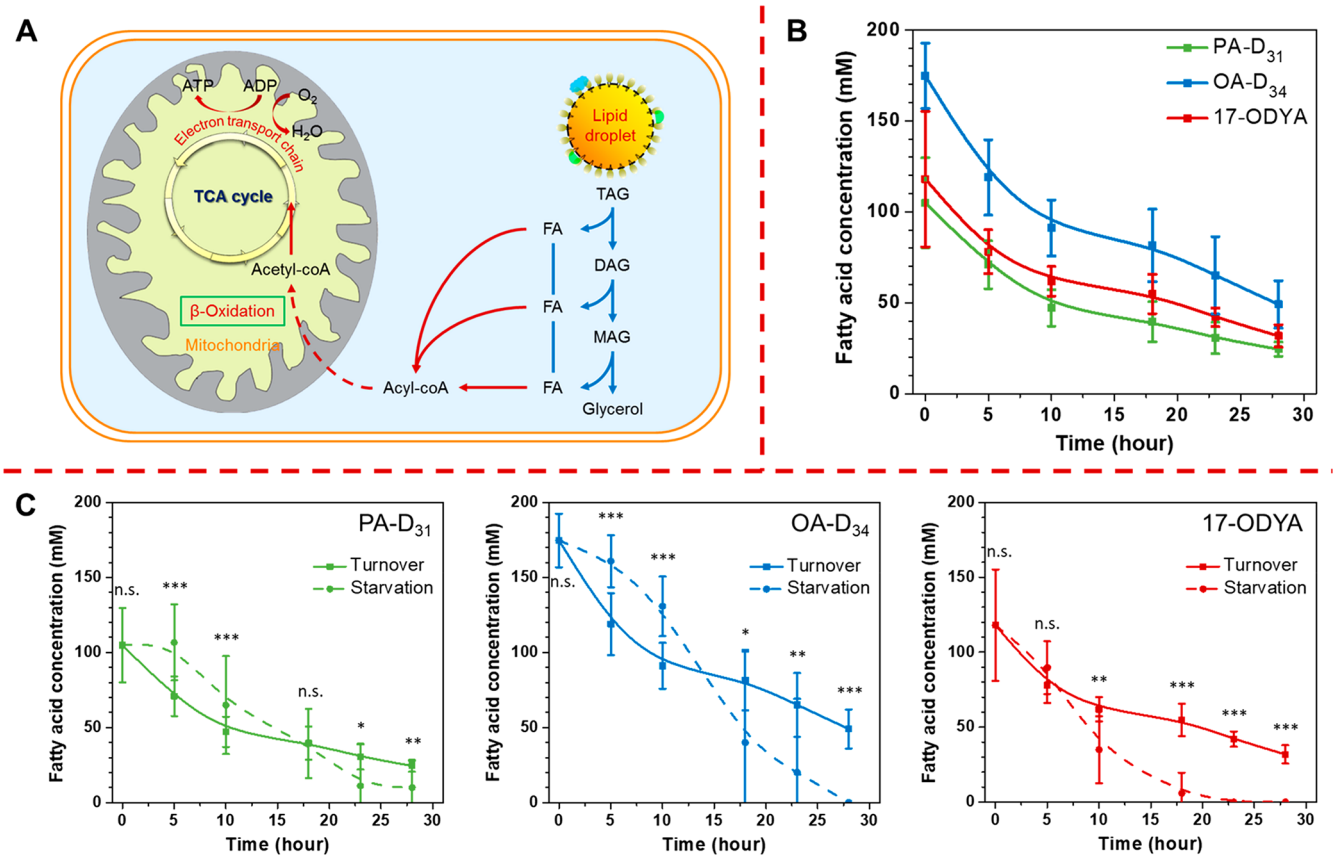

Figure 5. Tracing the basal fat turnover and lipolysis dynamics during starvation of different bioorthogonal fatty acids in wild-type *C. elegans*. (A) Scheme of lipid turnover and lipolysis pathways in eukaryotic cells (blue, stepwise hydrolysis of TAG to yield fatty acids; red, fatty acid derivatives can be imported into mitochondria for β-oxidation to generate acetyl-coA). (B) Quantitative measurement of basal fat turnover dynamics of the labeled lipids in the anterior region of worms ($n > 12$). (C) Basal fat turnover versus lipid consumption of the labeled lipids during starvation over different incubation times. Data are represented as mean ± SD. Unpaired, two-tailed *t* test was performed to determine significance. *, $P < 0.05$; **, $P < 0.01$; ***, $P < 0.001$.

hsSRS Imaging of LDs in *C. elegans*. Because fatty acid synthesis pathways are complex and not fully understood, we explored whether in vivo hsSRS imaging could produce information to understand the fatty acid desaturation/saturation.[21,33] We analyzed the composition of intestinal LDs of *C. elegans*, which were labeled with PA-D_{31} or OA-D_{34} for 25 h. By sequential spectral tuning of the Raman shift frame by frame, 75 images of wild-type worms were recorded at the C−D vibrational region from 2000 to 2300 cm^{-1} with a fine step size of 4 cm^{-1} (Supporting Information, Movie S3 and Movie S4). To compare the spectral lineshapes, all the hsSRS spectra were normalized to the C−D peak at 2117 cm^{-1}, as shown in Figure 6. Then the "unsaturation index" $R_{2252/2117}$ was defined by the ratio of SRS intensity at 2252 cm^{-1} for unsaturated ═C−D to that at 2117 cm^{-1} for saturated C−D (I_{2252}/I_{2117}).[33,52] Meanwhile, the control group of warms without any labeling showed a very flat Raman spectrum in the same vibrational region (Supporting Information, Movie S5 and Figure S29).

As shown in Figure 6A, the unsaturation index of worms fed with PA-D_{31} ($R_{2252/2117}$ = 16.7%) was found to be significantly higher than that of the PA-D_{31} pure solution ($R_{2252/2117}$ = 4.9%) and lower than the unsaturation index of the OA-D_{34} pure solution ($R_{2252/2117}$ = 24.7%) (Figure 6B). This intuitively demonstrated that the PA-D_{31} had been partially desaturated

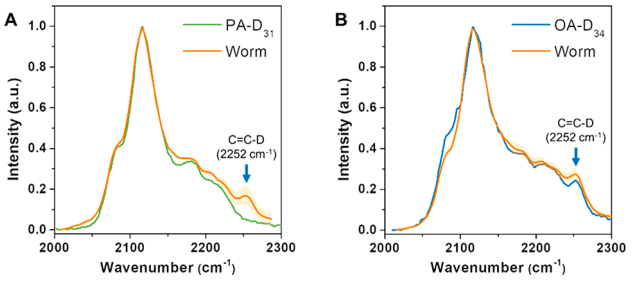

Figure 6. HsSRS spectra of intestinal LDs in wild-type *C. elegans* labeled with deuterated fatty acids versus that of pure solutions. Worms were fed with (A) PA-D_{31} or (B) OA-D_{34} for 25 h (n = 3). All hsSRS signals were normalized by the C−D peak at 2117 cm^{-1}, and the SRS intensity at 2252 cm^{-1} of C═C−D bonds exhibit increments for both curves marked with arrow. Shading along the line represents the standard deviation. See also Supporting Information, Movie S3, and Movie S4.

in the worms and the overall degree of unsaturation was between palmitic acid (C16:0) and oleic acid (C18:1n9).

Similarly, the unsaturation index of worms fed with OA-D_{34} ($R_{2252/2117}$ = 27.4%) was higher than that of the OA-D_{34} pure solution (Figure 6B), indicating that OA-D_{34} has been partially transformed into polyunsaturated fatty acids (PUFAs). Different from humans and many other species which have relatively large amounts of SFAs, PUFAs constitute a large proportion of

DOI: 10.1021/acs.analchem.8b04875
Anal. Chem. XXXX, XXX, XXX−XXX

fatty acids in *C. elegans*. In lab-used bacteria, only saturated and monounsaturated fatty acids (MUFAs) exist.[39] Thus, the PUFAs should be synthesized by a group of desaturases in *C. elegans*.[47] Overall, the results provide evidence that the bioorthogonal fatty acids used in this study can be effectively channeled into lipid metabolic pathways, showing their outstanding biocompatibility. The hsSRS imaging holds the potential to provide a new method for studying lipid conversion in vivo.

CONCLUSION

In this work, we developed a quantitative SRS imaging technique to determine the equivalent concentration of Raman bioorthogonal fatty acids in *C. elegans* in vivo. Owing to the narrow vibrational bands of Raman tags in the cell-silent region, we could obtain their genuine SRS intensity ($I_{SRS} = I_{ON} - I_{OFF}$) by subtracting the off-resonant non-Raman baseline (I_{OFF}) from the on-resonant SRS peak signal (I_{ON}). This method was demonstrated to efficiently suppress the non-Raman interference (e.g., LROs) and be capable of imaging the analyte of interest with high image contrast and quantitative determination in molar concentration. Because of the inertness of the SRS signal to environmental change, the extracellularly built calibrations could be used for determining the intracellular concentration of the analyte of interest under the same measurement conditions. However, the *C. elegans* samples could potentially scatter SRS signals, leading to an underestimation of our measurements. To this end, we measured SRS signals emitted by exogenous heavy water and olive oil with or without a worm in the optical path of SRS beam. The results demonstrate that such scattering loss caused by *C. elegans* was about 10% (Supporting Information, Movie S6, Movie S7, and Figure S30). This technique is of great importance for quantitative biochemical research because it can potentially facilitate the direct comparison of the results from the research conducted at different laboratories regardless of their parameter settings of SRS microscope. To demonstrate quantitative imaging of specific lipid metabolic process in vivo, we imaged, monitored, and quantified the alkyne-tagged fatty acid 17-ODYA, deuterium-labeled saturated and unsaturated fatty acids PA-D_{31}, and OA-D_{34} in live *C. elegans*. The molar concentration analyses clearly demonstrate that different lipid molecules show great differences in their incorporation and lipolysis dynamics, suggesting that the lipid-synthesizing enzymes in *C. elegans* have preference for their substrates.[48] Additionally, our work shows that hsSRS together with deuterated fatty acids serve as a promising tool to non-invasively study lipid desaturation in vivo. To the best of our knowledge, this was the first time that the desaturation of exogenous fatty acids was visualized in live animal. Our findings in the lipid metabolism, which are highly consistent with the previous reported results, demonstrate the powerful capability of the hsSRS microscope in quantitative analysis of lipid synthesis and lipolysis in vivo.

Besides lipids, C−D and alkyne labeling together with hsSRS have proved promising in imaging of specific metabolic activities of other molecules such as DNA, RNA, protein, and even glucose.[53,54] The excellent spectral specificity and outstanding biocompatibility of bioorthogonal labels open a new window to directly visualize the dynamics of these biological processes. Further development of hsSRS technique with fast-wavelength sweeping should enable more applications in quantitative monitoring of complex metabolism.

ASSOCIATED CONTENT

Supporting Information

The Supporting Information is available free of charge on the ACS Publications website at DOI: 10.1021/acs.analchem.8b04875.

Detailed system setup, hyperspectral imaging method, two-wavelength SRS subtraction method, system resolution, theoretical calculations, SRS and TPEF images and data analysis (PDF)

Z-Scanning SRS images of wild-type *C. elegans* at 2863 cm^{-1} CH_2 channel from different depths (1 μm/step) (AVI)

Z-Scanning SRS images of wild-type *C. elegans* at 2117 cm^{-1} PA-D_{31} channel from different depths (1 μm/step) (AVI)

hsSRS images of intestinal LDs in wild-type *C. elegans* labeled with PA-D_{31} for 25 h versus that of PA-D_{31} pure solution. (AVI)

hsSRS images of intestinal LDs in wild-type *C. elegans* labeled with OA-D_{34} for 25 h versus that of OA-D_{34} pure solutions (AVI)

hsSRS images of intestinal LDs in wild-type *C. elegans* without any labeling (control) (AVI)

Z-Scan SRS imaging of heavy water (2496 cm^{-1}) in which wild-type *C. elegans* has been submerged (5 μm/step). (AVI)

Z-Scan SRS imaging of olive oil (2863 cm^{-1}) in which wild-type *C. elegans* has been submerged (5 μm/step) (AVI)

AUTHOR INFORMATION

Corresponding Authors

*J.Y.Q.: E-mail, eequ@ust.hk.
*H.Y.M.: E-mail, hym@ust.hk.

ORCID

Xuesong Li: 0000-0002-1795-4885
Meijuan Jiang: 0000-0002-7918-7538
Congping Chen: 0000-0001-9186-4346
Zhongya Qin: 0000-0003-3899-2466
Ben Zhong Tang: 0000-0002-0293-964X
Jianan Y. Qu: 0000-0002-6809-0087

Author Contributions

⊥X.L., Y.L., and M.J. contributed equally to this work.

Notes

The authors declare no competing financial interest.

ACKNOWLEDGMENTS

J.Y.Q. acknowledges the financial support by the Hong Kong Research Grants Council through grants 662513, 16103215, 16148816, T13-607/12R, AOE/M-09/12, and C6002-17GF and Hong Kong University of Science & Technology (HKUST) through grant RPC10EG33. H.Y.M. acknowledges the financial support by the Hong Kong Research Grants Council through grant 662013 and HKUST through grant IGN12SC04.

REFERENCES

(1) Calder, P. C. *JPEN, J. Parenter. Enteral Nutr.* **2015**, *39*, 18S−32S.
(2) Walther, T. C.; Farese, R. V., Jr *Annu. Rev. Biochem.* **2012**, *81*, 687−714.

DOI: 10.1021/acs.analchem.8b04875
Anal. Chem. XXXX, XXX, XXX−XXX

(3) Greenberg, A. S.; Coleman, R. A.; Kraemer, F. B.; McManaman, J. L.; Obin, M. S.; Puri, V.; Yan, Q.-W.; Miyoshi, H.; Mashek, D. G. *J. Clin. Invest.* **2011**, *121* (6), 2102−2110.
(4) Röhrig, F.; Schulze, A. *Nat. Rev. Cancer* **2016**, *16* (11), 732−750.
(5) Matyash, V.; Liebisch, G.; Kurzchalia, T. V.; Shevchenko, A.; Schwudke, D. *J. Lipid Res.* **2008**, *49* (5), 1137−1146.
(6) Zhang, S. O.; Box, A. C.; Xu, N.; Le Men, J.; Yu, J.; Guo, F.; Trimble, R.; Mak, H. Y. *Proc. Natl. Acad. Sci. U. S. A.* **2010**, *107* (10), 4640−4645.
(7) Yen, K.; Le, T. T.; Bansal, A.; Narasimhan, S. D.; Cheng, J.-X.; Tissenbaum, H. A. *PLoS One* **2010**, *5* (9), No. e12810.
(8) Zhang, P.; Na, H.; Liu, Z.; Zhang, S.; Xue, P.; Chen, Y.; Pu, J.; Peng, G.; Huang, X.; Yang, F.; Xie, Z.; Xu, T.; Xu, P.; Ou, G.; Zhang, S. O.; Liu, P. *Mol. Cell. Proteomics* **2012**, *11* (8), 317−328.
(9) Watts, J. L. *Trends Endocrinol. Metab.* **2009**, *20* (2), 58−65.
(10) Wang, M. C.; Min, W.; Freudiger, C. W.; Ruvkun, G.; Xie, X. S. *Nat. Methods* **2011**, *8* (2), 135−138.
(11) Frøkjær-Jensen, C.; Davis, M. W.; Hopkins, C. E.; Newman, B. J.; Thummel, J. M.; Olesen, S.-P.; Grunnet, M.; Jorgensen, E. M. *Nat. Genet.* **2008**, *40*, 1375−1383.
(12) Hamada, K.; Fujita, K.; Smith, N. I.; Kobayashi, M.; Inouye, Y.; Kawata, S. *J. Biomed. Opt.* **2008**, *13* (4), 044027.
(13) Nan, X.; Cheng, J.-X.; Xie, X. S. *J. Lipid Res.* **2003**, *44* (11), 2202−2208.
(14) Freudiger, C. W.; Min, W.; Saar, B. G.; Lu, S.; Holtom, G. R.; He, C.; Tsai, J. C.; Kang, J. X.; Xie, X. S. *Science* **2008**, *322* (5909), 1857−1861.
(15) Saar, B. G.; Freudiger, C. W.; Reichman, J.; Stanley, C. M.; Holtom, G. R.; Xie, X. S. *Science* **2010**, *330* (6009), 1368−1370.
(16) Gluchowski, N. L.; Becuwe, M.; Walther, T. C.; Farese, R. V., Jr *Nat. Rev. Gastroenterol. Hepatol.* **2017**, *14* (6), 343−355.
(17) Freudiger, C. W.; Min, W.; Holtom, G. R.; Xu, B.; Dantus, M.; Xie, X. S. *Nat. Photonics* **2011**, *5*, 103−109.
(18) Wang, P.; Liu, B.; Zhang, D.; Belew, M. Y.; Tissenbaum, H. A.; Cheng, J. X. *Angew. Chem., Int. Ed.* **2014**, *53* (44), 11787−11792.
(19) van Manen, H.-J.; Lenferink, A.; Otto, C. *Anal. Chem.* **2008**, *80* (24), 9576−9582.
(20) Bergner, G.; Albert, C. R.; Schiller, M.; Bringmann, G.; Schirmeister, T.; Dietzek, B.; Niebling, S.; Schlücker, S.; Popp, J. *Analyst* **2011**, *136* (18), 3686−3693.
(21) Matthäus, C.; Krafft, C.; Dietzek, B.; Brehm, B. R.; Lorkowski, S.; Popp, J. r. *Anal. Chem.* **2012**, *84* (20), 8549−8556.
(22) Shen, Y.; Xu, F.; Wei, L.; Hu, F.; Min, W. *Angew. Chem., Int. Ed.* **2014**, *53* (22), 5596−5599.
(23) Wei, L.; Shen, Y.; Xu, F.; Hu, F.; Harrington, J. K.; Targoff, K. L.; Min, W. *ACS Chem. Biol.* **2015**, *10* (3), 901−908.
(24) Yamakoshi, H.; Dodo, K.; Okada, M.; Ando, J.; Palonpon, A.; Fujita, K.; Kawata, S.; Sodeoka, M. *J. Am. Chem. Soc.* **2011**, *133* (16), 6102−6105.
(25) Yamakoshi, H.; Dodo, K.; Palonpon, A.; Ando, J.; Fujita, K.; Kawata, S.; Sodeoka, M. *J. Am. Chem. Soc.* **2012**, *134* (51), 20681−20689.
(26) Wei, L.; Hu, F.; Shen, Y.; Chen, Z.; Yu, Y.; Lin, C.-C.; Wang, M. C.; Min, W. *Nat. Methods* **2014**, *11* (4), 410−412.
(27) Hong, S.; Chen, T.; Zhu, Y.; Li, A.; Huang, Y.; Chen, X. *Angew. Chem., Int. Ed.* **2014**, *53* (23), 5827−5831.
(28) Chen, Z.; Paley, D. W.; Wei, L.; Weisman, A. L.; Friesner, R. A.; Nuckolls, C.; Min, W. *J. Am. Chem. Soc.* **2014**, *136* (22), 8027−8033.
(29) Wei, L.; Hu, F.; Chen, Z.; Shen, Y.; Zhang, L.; Min, W. *Acc. Chem. Res.* **2016**, *49* (8), 1494−1502.
(30) Tipping, W.; Lee, M.; Serrels, A.; Brunton, V.; Hulme, A. *Chem. Soc. Rev.* **2016**, *45* (8), 2075−2089.
(31) Wei, L.; Chen, Z.; Shi, L.; Long, R.; Anzalone, A. V.; Zhang, L.; Hu, F.; Yuste, R.; Cornish, V. W.; Min, W. *Nature* **2017**, *544* (7651), 465−470.
(32) Slipchenko, M. N.; Le, T. T.; Chen, H.; Cheng, J.-X. *J. Phys. Chem. B* **2009**, *113* (21), 7681−7686.
(33) Fu, D.; Yu, Y.; Folick, A.; Currie, E.; Farese, R. V., Jr; Tsai, T.-H.; Xie, X. S.; Wang, M. C. *J. Am. Chem. Soc.* **2014**, *136* (24), 8820−8828.
(34) Stiebing, C.; Meyer, T.; Rimke, I.; Matthäus, C.; Schmitt, M.; Lorkowski, S.; Popp, J. *J. Biophotonics* **2017**, *10* (9), 1217−1226.
(35) Yu, Y.; Mutlu, A. S.; Liu, H.; Wang, M. C. *Nat. Commun.* **2017**, *8*, 865.
(36) Shen, Y.; Zhao, Z.; Zhang, L.; Shi, L.; Shahriar, S.; Chan, R. B.; Di Paolo, G.; Min, W. *Proc. Natl. Acad. Sci. U. S. A.* **2017**, *114* (51), 13394−13399.
(37) McCamant, D. W.; Kukura, P.; Mathies, R. A. *Appl. Spectrosc.* **2003**, *57* (11), 1317−1323.
(38) Zhang, D.; Slipchenko, M. N.; Leaird, D. E.; Weiner, A. M.; Cheng, J.-X. *Opt. Express* **2013**, *21* (11), 13864−13874.
(39) Gao, A. W.; Chatzispyrou, I. A.; Kamble, R.; Liu, Y. J.; Herzog, K.; Smith, R. L.; van Lenthe, H.; Vervaart, M. A.; van Cruchten, A.; Luyf, A. C.; van Kampen, A.; Pras-Raves, M. L.; Vaz, F. M.; Houtkooper, R. H. *Sci. Rep.* **2017**, *7*, 2408.
(40) Charron, G.; Zhang, M. M.; Yount, J. S.; Wilson, J.; Raghavan, A. S.; Shamir, E.; Hang, H. C. *J. Am. Chem. Soc.* **2009**, *131* (13), 4967−4975.
(41) Yount, J. S.; Moltedo, B.; Yang, Y.-Y.; Charron, G.; Moran, T. M.; López, C. B.; Hang, H. C. *Nat. Chem. Biol.* **2010**, *6* (8), 610−614.
(42) Li, X.; Lam, W. J.; Cao, Z.; Hao, Y.; Sun, Q.; He, S.; Mak, H. Y.; Qu, J. Y. *J. Biomed. Opt.* **2015**, *20* (11), 110501−110501.
(43) Li, X.; Jiang, M.; Lam, J. W.; Tang, B. Z.; Qu, J. Y. *J. Am. Chem. Soc.* **2017**, *139* (47), 17022−17030.
(44) Everall, N. J. Raman Spectroscopy of the Condensed Phase. In *Handbook of Vibrational Spectroscopy*; Griffiths, P., Chalmers, J. M., Eds.; John Wiley & Sons: London, 2002.
(45) McHale, J. L. *Molecular Spectroscopy*; CRC Press: Boca Raton, FL, 2017.
(46) Brock, T. J.; Browse, J.; Watts, J. L. *PLoS Genet.* **2006**, *2*, No. e108.
(47) Watts, J. L.; Browse, J. *Proc. Natl. Acad. Sci. U. S. A.* **2002**, *99* (9), 5854−5859.
(48) Man, W. C.; Miyazaki, M.; Chu, K.; Ntambi, J. *J. Lipid Res.* **2006**, *47* (9), 1928−1939.
(49) Nguyen, T. B.; Louie, S. M.; Daniele, J. R.; Tran, Q.; Dillin, A.; Zoncu, R.; Nomura, D. K.; Olzmann, J. A. *Dev. Cell* **2017**, *42* (1), 9−21.
(50) Chitraju, C.; Mejhert, N.; Haas, J. T.; Diaz-Ramirez, L. G.; Grueter, C. A.; Imbriglio, J. E.; Pinto, S.; Koliwad, S. K.; Walther, T. C.; Farese, R. V., Jr *Cell Metab.* **2017**, *26* (2), 407−418.
(51) Eichmann, T. O.; Kumari, M.; Haas, J. T.; Farese, R. V.; Zimmermann, R.; Lass, A.; Zechner, R. *J. Biol. Chem.* **2012**, *287* (49), 41446−57.
(52) Li, J.; Condello, S.; Thomes-Pepin, J.; Ma, X.; Xia, Y.; Hurley, T. D.; Matei, D.; Cheng, J.-X. *Cell Stem Cell* **2017**, *20* (3), 303−314.
(53) Li, J.; Cheng, J.-X. *Sci. Rep.* **2015**, *4*, 6807.
(54) Hu, F.; Chen, Z.; Zhang, L.; Shen, Y.; Wei, L.; Min, W. *Angew. Chem.* **2015**, *127* (34), 9959−9963.

DOI: 10.1021/acs.analchem.8b04875
Anal. Chem. XXXX, XXX, XXX−XXX